Journal of Thermal Analysis and Calorimetry, Vol. 76 (2004) 353–365

PHASE BEHAVIOR OF A THERMOTROPIC CUBIC MESOGEN 4'-*n*-HEXADECYLOXY-3'-NITRO-BIPHENYL-4-CARBOXYLIC ACID UNDER PRESSURE*

Y. Maeda[1**] *and S. Kutsumizu*[2]

[1]Nanotechnology Research Institute, National Institute of Advanced Industrial Science and Technology, Higashi 1-1, Tsukuba, Ibaraki 305-8565, Japan
[2]Department of Chemistry, Faculty of Engineering, Gifu University, Yanagido 1-1, Gifu 501-1193, Japan

Abstract

The phase behavior of an optically isotropic cubic mesogen 4'-*n*-hexadecyloxy-3'-nitrobiphenyl-4-carboxylic acid (ANBC-16) was investigated under hydrostatic pressures up to 200 MPa using a high-pressure DTA, a polarizing optical microscope equipped with a high-pressure hot-stage and a wide-angle X-ray diffractometer equipped with a high-pressure vessel. In the *T vs*. *P* phase diagram constructed in the heating mode, a triple point exists at 54±1 MPa and 205±1°C for the SmC, cubic, and SmA phases. A new mesophase, denoted here as X, appears in place of the cubic phase under pressures above about 60 MPa, while the X phase appears on cooling in the whole pressure region studied. Thus the X phase is a monotropic (metastable) phase between the SmA and Cub phases in the low pressure region, while being an enantiotropic phase between the SmA and SmC phases in the high pressure range. The X phase exhibits broken-fan or sand-like textures under pressure and a spot-like diffraction pattern, indicating the birefringent feature and no layered structure. It is suggested that the X phase is tetragonal or hexagonal columnar phase.

Keywords: ANBC-16, high-pressure DTA, pressure-induced mesophase, thermotropic cubic mesogen, triple point, *T vs. P* phase diagram

Introduction

Thermotropic cubic mesogens have been attracting considerable scientific interests because they are optically isotropic. In 1957, a homologous series of mesomorphic 4'-*n*-alkoxy-3'-nitrobiphenyl-4-carboxylic acids, ANBC-*n*, where *n* is the number of carbon atoms in the alkoxy chain, was synthesized by Gray *et al.* [1]. Demus *et al*. [2] gave evidence for the thermotropic cubic mesophase of the ANBC-16 and ANBC-18. ANBC-*n* homologues is one of the most fascinating phases in the liquid crystalline systems in that some types of rod-like molecules form an optically isotropic structure in a temperature range sandwiched by other anisotropic phases with lamellar, hexag-

* This paper is dedicated to Prof. Karasz to salute him on his 70's birthday
** Author for correspondence: E-mail: yoji.maeda@aist.go.jp

1388–6150/2004/ $ 20.00

Akadémiai Kiadó, Budapest
Kluwer Academic Publishers, Dordrecht

onal, or columnar structures [3, 4]. The stability of the cubic phase for the ANBC-*n* series is strongly dependent upon the length *n* of the alkoxy groups. The ANBC-*n* homologues show the cubic phase for $n>15$ (and up to 26 at present) and over a temperature range which becomes broader, essentially, with increasing *n* [5]. ANBC-16 exhibits substantially the crystal (Cr) – smectic C (SmC) – cubic (Cub) – smectic A (SmA) – isotropic liquid (I) transition sequence under atmospheric pressure. In the solid and liquid crystalline phases, most of the ANBC-16 molecules are dimerized via intermolecular hydrogen bonds [6, 7], and thus the structural unit is the dimerized molecule that has an extended core of coupled nitrobiphenylcarboxylic acids at its center and two terminal alkoxy chains.

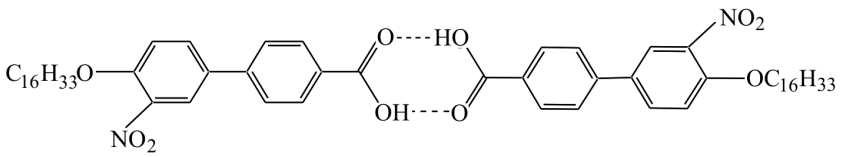

Tardieu and Billard [8] identified the space group *Ia3d* for the cubic phase of ANBC-16, and showed that the unit cell contains more than 1000 molecules of ANBC-16. They adopted the interwoven jointed-rod model, which was first postulated for the lyotropic *Ia3d* cubic phases by Luzzati and Spegt [9].

High-pressure investigation of the phase behavior of materials helps us to understand the structure-property relationship of crystalline and mesophase polymorphs [10, 11]. Shankar Rao *et al*. reported the interesting *T vs. P* phase diagram of ANBC-16 constructed by the measurements of transmitted light intensity on cooling under pressure [12]: the cubic phase disappears at about 40 MPa, while a columnar (Col) phase is formed between the SmA and SmC (or Cub in the low pressure region) phases under high pressures. The authors also studied the transition behavior of ANBC-16 using a high-pressure DTA and determined the *T* vs. *P* phase diagram on heating; this exhibits a triple point for the SmC, Cub and SmA phases [13]. The resulting phase diagram exhibits the disappearance of the cubic phase at about 65 MPa and the appearance of a new phase (X), in place of the cubic phase, between the SmC and SmA phases in the high pressure region. There is a significant difference in the two phase diagrams; their triple point is for the SmC, Cub and Col phases, and its phase diagram has the Cub–Col transition line with a negative slope (d*T*/d*P*), while no such transition line having a negative slope is in our diagram. The discrepancy of phase behavior and triple point of ANBC-16 encouraged us to reinvestigate the thermal behavior and in-situ observations of the texture and structure of ANBC-16 under hydrostatic pressure, especially focused on the phase behavior of the X phase. Recently the authors presented the analytical results of the thermal behavior and morphological texture of ANBC-16 under pressure and explained the discrepancy in the two phase diagrams [14, 15].

In this paper we review the experimental results on the phase transition of ANBC-16 measured using a high-pressure differential thermal analyzer (DTA), a polarizing optical microscope (POM) equipped with a high-pressure optical cell, and a

wide-angle X-ray diffraction apparatus equipped with a high-pressure vessel under hydrostatic pressures up to 200 MPa.

Experimental

Sample preparation

ANBC-16 was prepared according to the method by Gray *et al*. [1]. Samples were recrystallized from ethanol several times and the purity was confirmed by infrared (IR), ^{1}H NMR, mass spectroscopy (MS), and elemental analysis.

DTA measurements under pressure

The high pressure DTA apparatus used in this study is described elsewhere [16]. The DTA system was operated in a temperature range between room temperature and 250°C under hydrostatic pressure up to 200 MPa. Dimethylsilicone oil with a medium viscosity (100 cSt) was used as the pressurizing medium. The sample weighing about 4 mg was put in the DTA sample cell and coated with epoxy adhesives, in order to fix the sample to the bottom of the cell and also to prevent direct contact with the silicone oil. The DTA runs were performed at a constant scan rate of 5°C min^{-1} under various pressures. Transition temperatures were determined in the same manner as in the DSC analysis.

Polarized optical microscope measurements under pressure

Texture of ANBC-16 was observed using a Leitz Orthoplan polarizing optical microscope (POM) equipped with either a Mettler FP-82 hot stage or a high-pressure optical cell which is described precisely elsewhere [17]. Figure 1 shows the photograph of the total view of the high-pressure optical cell set on the stage of the optical microscope. Pressure and temperature were monitored simultaneously during the morphological observation. Two routes of procedure were adopted for the texture observa-

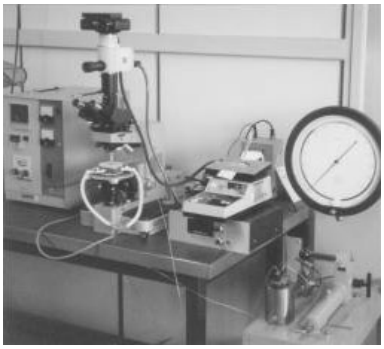

Fig. 1 Photograph of the polarizing optical microscope equipped with a high-pressure optical cell system

tion under hydrostatic pressure. Route one is an isobaric process: cooling and heating processes at 65 MPa, in which the X phase appears in place of the cubic phase between the SmC and SmA phases. Route two is an isothermal process at 185°C, which starts from the cubic phase at 5 MPa to the X phase at 65 MPa or more high pressure.

Wide-angle X-ray diffraction measurements under pressure

The high-pressure wide-angle X-ray diffraction (WAXD) apparatus used in this study is described elsewhere [16]. The high-pressure vessel was set on the wide-angle goniometer of 12 kW rotating anode X-ray generator (Rotaflex RU-200, Rigaku, Co.). The pressure vessel consists of a beryllium spindle as a sample cell, sandwiched between the upper and lower heater blocks. Dimethylsilicone oil of low viscosity (10 cSt) was used as the pressure medium. Sample was inserted into the vertical hole of the beryllium spindle. The beryllium spindle was mechanically sealed by the upper and lower heater blocks and then the sample was pressurized hydrostatically at pressures up to 200 MPa. Ni-filtered CuK_α X-ray was irradiated to the sample and the X-ray reflections were detected on the equatorial line using a curved PSPC detector (PSPC-30, Rigaku Co. Ltd). Each pattern was taken by counting a period of time for 200–300 s. Also the diffraction patterns were obtained using an imaging plate detector (BAS-IP 127×127 mm, Fuji Photo Film Co., Ltd.).

Results and discussion

Figure 2 shows the DSC curves of ANBC-16 at a scanning rate of 5°C min^{-1}. The heating curve exhibits three small endothermic peaks of the Cr_4–Cr_3, Cr_3–Cr_2 and Cr_2–Cr_1 transitions at 47.5, 74.5 and 89.4°C, a major peak of the Cr_1–SmC transition at 124.9°C, a small peak of the SmC–Cub transition at 175.1°C, double peaks of the

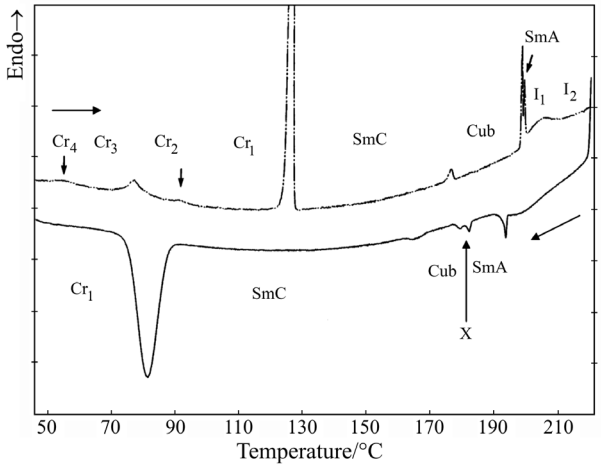

Fig. 2 DSC heating and cooling curves of ANBC-16. Scanning rate: 5°C min^{-1} (from [15], reproduced by permission of Taylor & Francis, Ltd.)

Cub–SmA and SmA–I_1 transitions at 197.9 and 198.8°C, and finally a broad peak of the 'ordered' isotropic liquid (I_1)–isotropic liquid (I_2) transition at 203.1°C. The I_1–I_2 transition is assigned to the dissociation of hydrogen-bonded dimers to the genuine isotropic liquid of isolated ANBC-16 molecules [6, 7]. As already reported, a very metastable mesophase is observed monotropically over a small temperature interval of 1–2°C between the SmA and Cub phases on cooling. The appearance of the metastable phase is related closely with the X phase observed under elevated pressures, which will be described in the later section. The reliable thermodynamic quantities associated with the phase transitions of ANBC-*n* homologues were measured

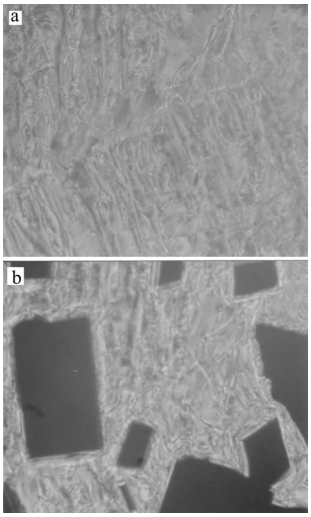

Fig. 3 POM photographs of a – SmC phase at 150°C and b – the texture associated with the SmC–Cub transition at 179°C at atmospheric pressure (from [13], reproduced by permission of Taylor & Francis, Ltd.)

by the precise calorimetric measurements [18–21]. Figure 3 shows the typical texture of (a) the SmC phase at 150°C, and (b) the texture associated with the SmC–Cub transition at 179°C, in which the black, isotropic area of the cubic phase have quite distinctive shapes–squares, rectangles and rhombic. These growing portions eventually coalesce to give a totally black field of an optically isotropic field.

Thermal behavior of ANBC-16 under pressure

Figure 4 shows the DTA heating curves of ANBC-16 in the pressure range up to 200 MPa. The DTA curves at low pressures correspond well with the DSC heating curve shown in Fig. 2, indicating the Cr_4–Cr_3–Cr_2–Cr_1–SmC–Cub–SmA–I_1–I_2 transition sequence. The stable temperature region of the cubic phase decreases with increasing pressure. Then the small peak of the SmC–Cub transition disappears, while a new endothermic peak appears at a lower temperature under high pressures. This phenomenon indicates that a new mesophase, denoted here as X, appears in place of

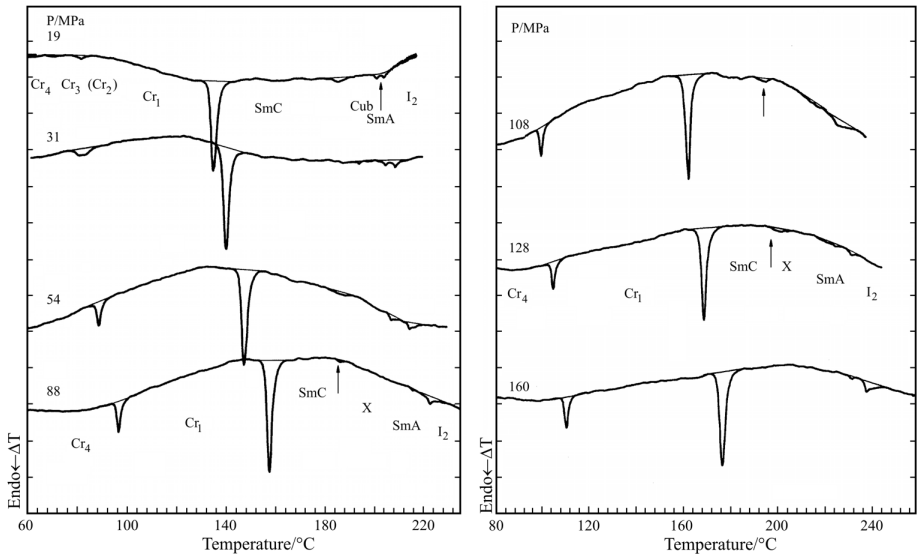

Fig. 4 DTA heating curves of ANBC-16 under various pressures (from [13], reproduced by permission of Taylor & Francis, Ltd.)

the cubic phase between the SmC and SmA phases under high pressures. The transition sequence on heating at high pressure can be described as

$$Cr_4–Cr_1–SmC–X–SmA–I_1–I_2.$$

The *T vs. P* phase diagram of ANBC-16 constructed in the heating mode is shown in Fig. 5. There are several interesting features in the phase diagram. Firstly, the cubic phase disappears under elevated pressures above about 60 MPa. At the same time, secondly, the X phase in place of the cubic phase is formed between the SmC and SmA phases at higher pressures. The X phase corresponds to the columnar phase noted by Shankar Rao *et al.*, only in the high pressure region, but the X phase cannot be detected in the pressure range between 0.1 and 60 MPa. Third, the *T vs. P* phase diagram in Fig. 5 shows a boundary region between the low and high pressure regions, as shown by the dotted lines. Shankar *et al*. reported the *T vs. P* phase diagram constructed in the cooling mode by an optical method [12]. In their phase diagram the columnar phase exists between the cubic and SmA phases in the low pressure region. There is a substantial difference of triple point in the two phase diagrams: their triple point is for the SmC, Cub and Col phases, while the triple point here is for the SmC, Cub, and SmA phases. Their Cub–Col transition line has a negative slope (d*T*/d*P*) with pressure, while the phase diagram (Fig. 5) has no transition line with a negative slope. So the thermal behavior of ANBC-16 was reexamined on heating and subsequent cooling processes under pressures up to 150 MPa, to analyze the phase behavior of the X phase and to compare the results with the Shankar *et al*.'s phase diagram.

The DTA heating curve at 27 MPa shows the same behavior as shown in Fig. 4, indicating the Cr_4–Cr_3–(Cr_2)–Cr_1–SmC–Cub–SmA–I_1–I_2 transition sequence. On the subsequent cooling from the I_1 phase, however, four small exothermic peaks, attributable to the $I_1 \rightarrow$SmA, SmA$\rightarrow$X, X Cub, and Cub SmC transitions in the order of decreasing temperature, were slightly observed in the high temperature region. Accordingly the transition sequence I_1–SmA–X–Cub–SmC–Cr_1–Cr_4 is recognized on cooling at 27 MPa. The additional X phase between the peaks of the SmA–X and X–Cub transitions was observed on cooling at other low pressures. Accordingly the X phase appears monotropically and so it is metastable. Figure 6 shows the DTA heating and subsequent cooling curves of ANBC-16 at 100 MPa. As reported before,

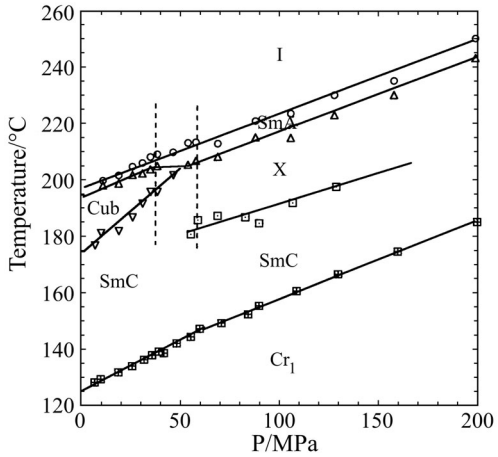

Fig. 5 *T vs. P* phase diagram of ANBC-16 constructed in the heating mode (from [15], reproduced by permission of Taylor & Francis, Ltd.)

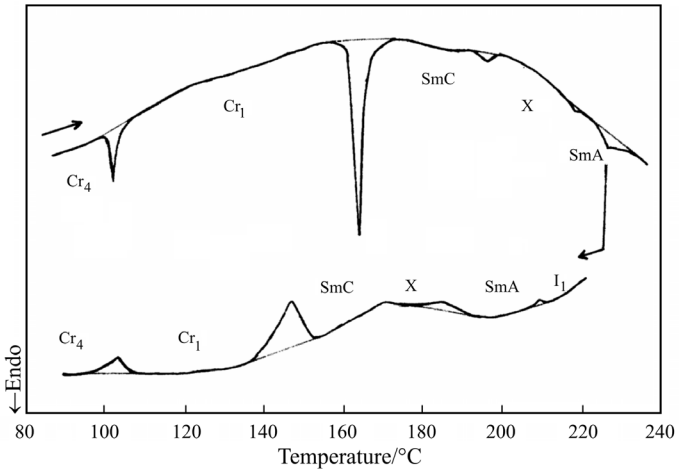

Fig. 6 DTA heating and cooling curves of ANBC-16 at 100 MPa (from [15], reproduced by permission of Taylor & Francis, Ltd.)

the X phase appears reversibly in place of the cubic phase at high pressures, indicating the Cr_4–Cr_1–SmC–X–SmA–I_1–I_2 transition sequence. The X phase appears

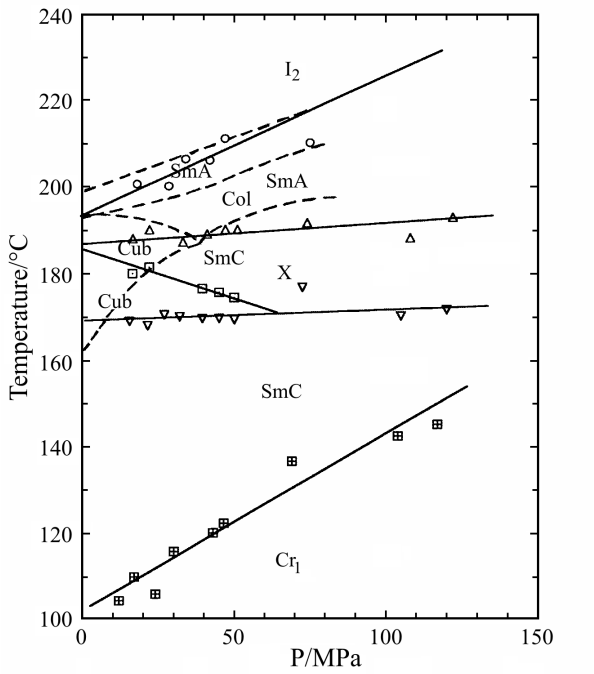

Fig. 7 *T vs. P* phase diagrams of ANBC-16 constructed in the cooling mode. The *T vs. P* phase diagram by Shankar Rao *et al*. are drawn as dotted curves for comparison

enantiotropically at 100 MPa. Figure 7 shows the *T vs. P* phase diagram for ANBC-16 constructed in the cooling mode. The transition curves can be approximated as first order polynomials in terms of pressure. An important feature of the *T vs. P* phase diagram constructed in the cooling mode is the appearance of the X phase in the whole pressure region. Combining with the phase diagram in Fig. 5, the X phase is found to be enantiotropic under pressures above about 60 MPa, while it is monotropic under lower pressures. The enantiotropic X phase in the high-pressure region has a temperature width of about 20°, while the temperature range of the monotropic X phase at low pressures below 60 MPa becomes narrow with decreasing pressure, due to the appearance of the cubic phase. The X→Cub transition line has a negative slope (dT/dP=–17°C/100 MPa), while all the other transition lines have positive slopes. The monotropic X phase has a possibility of appearing under atmospheric pressure, as suggested by the extrapolation of the SmA–X and X–Cub transition lines to the ordinate. This possibility is supported by the appearance of a monotropic mesophase on the DSC cooling curve, as shown in Fig. 2. As is shown by the

dotted curves for the Shankar *et al.*'s phase diagram, the *T vs. P* phase diagram constructed in the cooling mode is similar to their phase diagram [12], although the transition points and the transition curves are considerably drifted. So the X phase in this study is the same one as their Col phase. The X–Cub transition line crosses over the Cub–SmC transition line at about 65 MPa, leading to a triple point for the SmC, Cub and X(Col) phases. It should be noted, however, that the monotropic X phase is not thermodynamically stable.

Table 1 Thermodynamic quantities associated with the phase transitions of ANBC-16

Phase transition	T/°C	ΔH/ kJ mol^{-1}	ΔS/ J mol^{-1} K^{-1}	$(dT/dP)_{1atm}$	ΔV/ cm^3 mol^{-1}
$Cr_1 \rightarrow SmC$	398.2	38.6	96.9	0.350_2	33.9
$SmC \rightarrow Cub$	447.7	0.5	1.1	0.591_0	0.6_5
$Cub \rightarrow SmA$	471.1	1.5	3.2	0.258_5	0.8
$SmA \rightarrow I_1$	472.0	0.9	1.9	0.248_2	0.5

The ΔV value of each transition was calculated using the Clausius–Clapeyron equation $dT/dP=\Delta V/\Delta S=T\Delta V/\Delta H$

The thermodynamic quantities associated with the phase transitions of ANBC-16 are listed in Table 1. Since all of the transition enthalpies and slopes (dT/dP) of the transitions are positive, all the ΔV values of the transitions calculated using the Clausius–Clapeyron equation are positive. The positive sign for the SmC–Cub transition suggests that the molar volume for the cubic phase is larger than that of the SmC phase. In fact, the experimental fact of the volume change of ANBC-22 supports this suggestion [22]. It is noted that the transition entropy and the transition volume for the SmC–Cub transition are only 1–2% of the total transition entropies and volumes.

Morphological and structural characterization of ANBC-16 under pressure

The same morphological features of ANBC-16 as those observed at atmospheric pressure were recognized under pressures up to 40 MPa, although the cubic and isotropic liquid phases show the dark brown, not black, field of view under hydrostatic pressure. The SmC–Cub transition is recognized clearly under pressure because the dark brown field of view for the cubic phase changes into the birefringent texture of the SmC phases. It is intriguing to study the morphological and structural characterization of the X phase under pressure. Figure 8 displays the POM photographs of the texture of ANBC-16 on cooling from the isotropic liquid at 65 MPa. The focal conic texture of the SmA phase appears in the isotropic liquid at 200°C, Fig. 8a, and the texture grows in the whole field of view at 199°C, Fig. 8b. On cooling, the change in texture is observed at 195°C, Fig. 8c, indicating the breaking of the focal conic fan texture. Then the broken-fan texture for the X phase is observed at 190°C, Fig. 8d, and the texture is maintained in the SmC phase at 135°C, Fig. 8e. The texture of the SmC phase, quite similar to those for the X phase, is observed until the crystallization

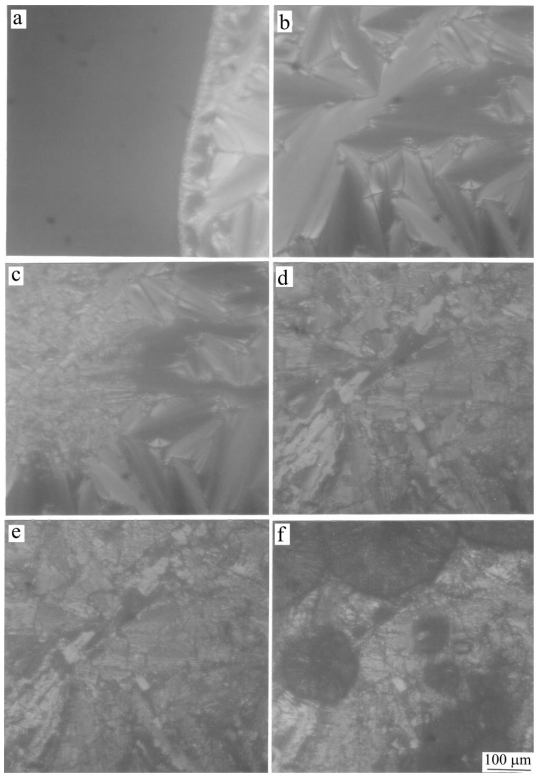

Fig. 8 POM photographs of the textures of ANBC-16 on cooling from the isotropic liquid at 65 MPa: a – the SmA phase growing in the dark field of the isotropic liquid at 200°C; b – focal conic texture for the SmA phase at 199°C; c – breaking of the focal conic texture during the SmA–X transition at 195°C; d – plate-like broken-fan texture for the X phase at 190°C; e – broken-fan texture for the SmC phase at 135°C; and f – crystallization at 121°C (from [14], reproduced by permission of Taylor & Francis, Ltd.)

occurs at 121°C, Fig. 8f. The morphological observation was performed consecutively on the subsequent heating from 100°C at 65 MPa. The crystal spherulites are observed at temperatures up to ca. 140°C. After the Cr_1–SmC transition, the sand-like texture of the SmC phase is observed at temperatures up to about 185°C. The sand-like texture is maintained at 195°C beyond the SmC–X transition at 190°C, but the brightness changes abruptly. On further heating at 201°C, the texture shows partly the focal conic texture, characteristic of the SmA phase. Here it is noted that the optically isotropic cubic phase no longer appears on cooling and heating at 65 MPa. The morphological features for the X phase are clearly different from the cubic phase: the X phase is birefringent, similar to the SmC phase, while the cubic phase shows the optically isotropic, dark field of view. The texture of the X phase is clearly different from the rod-like batonnets or the mosaic textures for the S4 phase reported earlier [3]. It is interesting to see how the optically isotropic, dark field for

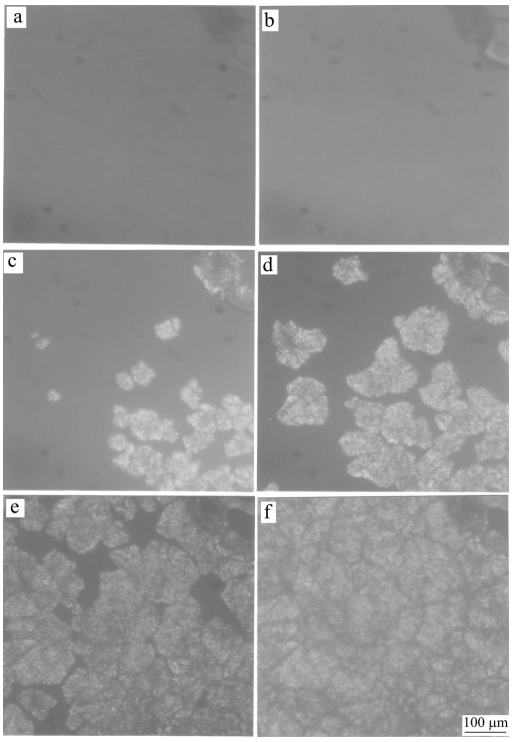

Fig. 9 POM photographs of the texture of ANBC-16 on pressurizing process from 5 to 65 MPa at 185°C: a – and b – optically isotropic, dark brown field for the cubic phase at 5 and 50 MPa; c – bright islands for the X phase in the dark field at 55 MPa; d – the same as c – taken after 5 min; e – bright islands coalesce to form a homogeneous texture for the X phase at 60 MPa; f – sand-like texture for the X phase at 65 MPa (from [14], reproduced by permission of Taylor & Francis, Ltd.)

the cubic phase changes by pressurizing process. Another POM experiment under pressure was performed along the isothermal path. The dark brown field of view for the cubic phase at 5 MPa, Fig. 9a, is the initial state of the pressurizing experiment at 185°C. The dark brown field of view is held at pressures up to 50 MPa, Fig. 9b. When pressure is raised to 55 MPa, small bright islands were formed sporadically in the dark field of the cubic phase, Fig. 9c, indicating the appearance of the X phase. The bright islands are grown for 5 min at 55 MPa, Fig. 9d, and the growth is accelerated at 60 MPa, Fig. 9e. The bright islands coalesce each other to form a homogeneous texture with many grain boundaries at 65 MPa, Fig. 9f. The bright sand-like texture of the X phase at 65 MPa is very similar to that of the SmC phase. The reversible change in texture was observed by decreasing pressure. The same morphological change during the Cub–X transition was recognized at 180 and 190°C.

The X-ray investigation for the cubic phase of ANBC-16 by Diele *et al*. shows two principal features in the diffraction pattern: a diffuse ring at 0.45 nm and a small number of sharp low angle reflections. Figure 10 shows the three WAXD patterns in

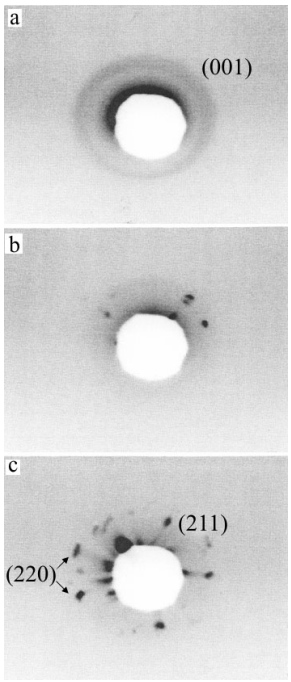

Fig. 10 WAXD patterns of ANBC-16 in the low-angle region: a – SmC phase at 165°C and 80 MPa; b – the X phase at 201°C and 80 MPa; c – cubic phase at 185°C and 1 atm (from [14], reproduced by permission of Taylor & Francis, Ltd.)

the low angle region of ANBC-16, measured (a) at 165°C and 80 MPa for the SmC phase, (b) at 201°C and 80 MPa for the X phase, and (c) at 185°C and atmospheric pressure for the cubic phase. The WAXD pattern of the X phase consists of several strong and weak spots, similar to that for the cubic phase. The spot-like pattern reflects the presence of relatively large domains, suggesting no layered structure for the X phase. The detailed analysis of the X-ray diffraction was performed by Tardieu and Billard [8]. The suggested molecular arrangement is quite analogous to the model for a lyotropic cubic phase proposed by Luzzati and Spegt [9]. The cubic phase of ANBC-16 is characterized with the space group having *Ia3d* and its unit cell contains a large number (more than 1000) of molecules [23, 24]. On the other hand, similar cubic phases are found in micro-phase separated systems such as lyotropic systems and block-copolymers. In these systems, the structures of cubic phases are characterized by the presence of triply periodic minimal surface (TPMS, or called infinitely periodic minimal surface, IPMS) as interface geometry [25]. The structure of the cubic phase of ANBC-*n* and other thermotropic cubic molecules is discussed in terms of the TPMS model.

Finally, it is emphasized that the cubic phase is destabilized with increasing pressure and disappears under high pressures above 60 MPa. It is concluded from the in-situ morphological and structural observations under pressure that the X phase is

an optically anisotropic, birefringent phase and that the structure of the X phase would be either tetragonal or hexagonal columnar phase.

References

1 G. W. Gray, B. Jones and F. Marson, J. Chem. Soc., (1957) 393.
2 D. Demus, G. Kunicke, J. Neelsen and H. Sackmann, Z. Naturforsch., 23a, (1968) 84.
3 G. W. Gray and J. W. Goodby, Smectic Liquid Crystals – Textures and Structures (Leonard Hill, Glasgow), Chap. 4 1984.
4 S. Diele and P. Göring, Handbook of Liquid Crystals, Ed. by D. Demus, J. Goodby, G. W. Gray, H.-W. Spiess and V. Vill, Wiley-VCH, Weinheim, 2B (1998) 887.
5 S. Kutsumizu, M. Yamada and S. Yano, Liq. Cryst., 16 (1994) 1109.
6 S. Kutsumizu, R. Kato, M. Yamada and S. Yano, J. Phys. Chem. B, 101 (1997) 1666.
7 M. Tansho, Y. Onoda, R. Kato, S. Kutsumizu and S. Yano, Liq. Cryst., 24 (1998) 525.
8 A. Tardieu and J. Billard, J. Phys. (Paris) Coll., 37 (1976) C3-79.
9 V. Luzzati and A. Spegt, Nature, 215 (1967) 701.
10 A. Morawski, K. Przybylski and T. Lada, J. Therm. Anal. Cal., 68 (2002) 243.
11 E. V. Boldyreva, T. P. Shakhtshneider, H. Ahsbahs, H. Sowa and H. Uchtmann, J. Therm. Anal. Cal., 68 (2002) 437.
12 D. S. Shankar Rao, S. Krishna Prasad, Veena Prasad and Sandeep Kumar, Phys. Rev. E., 59 (1999) 5572.
13 Y. Maeda, G.-P. Cheng, S. Kutsumizu and S. Yano, Liq. Cryst., 28 (2001) 1785.
14 Y. Maeda, S. Krishna Prasad, S. Kutsumizu and S. Yano, Liq. Cryst., 30 (2003) 7.
15 Y. Maeda, K. Morita and S. Kutsumizu, Liq. Cryst., 30 (2003) 157.
16 Y. Maeda and H. Kanetsuna, Bull. Res. Inst. Polym. Tex., 149 (1985) 119; Y. Maeda, Thermochim. Acta, 163 (1990) 211.
17 Y. Maeda and M. Koizumi, Rev. Sci. Instrum., 67 (1996) 2030; Y. Maeda, Y.-K. Yun and J.-I. Jin, Mol. Cryst. Liq. Cryst., 312 (1998) 223.
18 K. Saito, A. Sato and M. Sorai, Liq. Crsyt., 25 (1998) 525.
19 N. Morimoto, K. Saito, Y. Morita, K. Nakasuji and M. Sorai, Liq. Cryst., 26 (1999) 219.
20 A. Sato, K. Saito and M. Sorai, Liq. Cryst., 26 (1999) 341.
21 A. Sato, Y. Yamamura, K. Saito and M. Sorai, Liq. Cryst., 26 (1999) 1185.
22 S. Kutsumizu, M. Yamada, K. Tadano, S. Yano, S. Nojima and T. Yamaguchi, in press.
23 A.-M. Levelut and M. Clerc, Liq. Cryst., 24 (1998) 105.
24 P. Göring, S. Diele, S. Fischer, A. Wiegeleben, G. Pelzl, H. Stegemeyer and W. Thyen, Liq. Cryst., 25 (1998) 457.
25 K. Saito and M. Sorai, Chem. Phys. Lett., 366 (2002) 56.